Quantum Entropic Self-Localization with Ultracold Fermions

Mikhail Mamaev, Itamar Kimchi, Michael A. Perlin, Rahul M. Nandkishore, and Ana Maria Rey

Phys. Rev. Lett. **123**, 130402 — Published 27 September 2019

DOI: 10.1103/PhysRevLett.123.130402

Quantum entropic self-localization with ultracold fermions

Mikhail Mamaev,[1,2,3,*] Itamar Kimchi,[1,2,3] Michael A. Perlin,[1,2,3] Rahul M. Nandkishore,[2,3] and Ana Maria Rey[1,2,3]

[1] *JILA and NIST, University of Colorado, Boulder, CO 80309, USA*

[2] *Department of Physics, University of Colorado, Boulder, CO 80309, USA*

[3] *Center for Theory of Quantum Matter, University of Colorado, Boulder, CO 80309, USA*

(Dated: September 9, 2019)

We study a driven, spin-orbit coupled fermionic system in a lattice at the resonant regime where the drive frequency equals the Hubbard repulsion, for which non-trivial constrained dynamics emerge at fast timescales. An effective density-dependent tunneling model is derived, and examined in the sparse filling regime in 1D. The system exhibits entropic self-localization, where while even numbers of atoms propagate ballistically, odd numbers form localized bound states induced by an effective attraction from a higher configurational entropy. These phenomena occur in the strong coupling limit where interactions only impose a constraint with no explicit Hamiltonian term. We show how the constrained dynamics lead to quantum few-body scars and map to an Anderson impurity model with an additional intriguing feature of non-reciprocal scattering. Connections to many-body scars and localization are also discussed.

Introduction. Ultracold atomic systems loaded into optical lattices are among the most powerful quantum simulation platforms accessible today, especially when augmented with emerging capabilities for individual-particle manipulation. Dynamical control over internal and external degrees of freedom, lack of disorder, long coherence times and tunable interactions allow these systems to capture many of the ingredients at the heart of modern quantum science [1]. These include gauge fields [2], superconductivity [3], and even phenomena relevant to high-energy physics such as confinement [4]. However, optical lattice systems are often limited by slow effective cross-site interaction timescales such as superexchange in the Mott insulating regime.

In this work we look at a resonance-assisted model operating in the strongly interacting regime. This model gives rise to constrained physics where atomic motion is strongly correlated and species-dependent, while evolving at timescales set by the lattice tunneling rate. Our model employs a driving laser that interrogates internal pseudo-spin states, and imposes a relative phase between every lattice site which generates spin-orbit coupling (SOC) [5–8]. The competition between the SOC-inducing drive and interactions makes one tunneling process resonant and inhibits the other processes, yielding an effective density-dependent tunneling. This setup is connected to prior experiments using tilted [9–13] and shaken lattices [14–20] to study gauge fields [21–26], transport [27, 28], Mott-metal transitions [29] and many other phenomena [30]. Our work avoids the issue of heating effects caused by Floquet engineering, has a straightforward implementation, and explores subjects of scattering and localization that have not been considered as often in this context [31, 32]. This work is also related to the prior proposal of generating cluster states [33], but now explores the non-perturbative regime where conventional superexhange breaks down.

The density-dependent model we derive exhibits multibody self-localization, where particles localize themselves without additional external potentials. The effect is akin to a quantum entropic self-confinement, caused by the emergence of bound states induced by the minimization of kinetic energy in Fock states with higher connectivity. The bound states feature different physics than other mobile scattering states, a behavior that is reinforced by mapping the dynamics to an Anderson impurity model [34–36], allowing us to derive analytic results on bound populations and scattering coefficients. This mapping is also supplemented by a particular type of asymmetric behaviour similar to those found in nonreciprocal systems [37], manifesting as a scattering process where transmission moves a scatterer while reflection keeps it in place. These constrained dynamics are connected to the study of quantum scars [38–40] as closed trajectories arise depending on the boundaries, drastically changing the long-time density profiles. Our results are also similar to those seen in Efimov physics [41–43], since our system exhibits a three-body bound state and free-propagating two-body pairs. While the physics described here is at the level of a 1D system for which a hardcore boson description would yield equivalent results, the experimental implementation poses no significant restriction on dimension. This opens a wealth of prospects for further studies of even richer phenomena in higher dimensions, where Fermi statistics will matter and the features of quantum scars and non-reciprocity become qualitatively distinct.

The system can be realized experimentally in a number of platforms. The most promising one is 3D optical lattices using ultracold alkaline earth atoms, for which the long lifetimes and magnetic field insensitivity permit a clean study. Having faster timescales also permits implementation in systems with access to modern tools that allow for single-atom addressability, such as quantum gas microscopes [44–49] and optical tweezers [50–53], which would facilitate easier observation of the dynamics.

Model. Our starting point is a cubic optical lattice of L sites populated by N fermionic atoms with two internal pseudospin states g, e in the lowest Bloch band. The system is 3D in principle, although in this work we restrict to 1D by making the lattice confinement stronger along transverse directions. A resonant interrogating laser drives transitions between the internal states. The Hamiltonian is $\hat{H} = \hat{H}_0 + \hat{H}_\Omega$, where

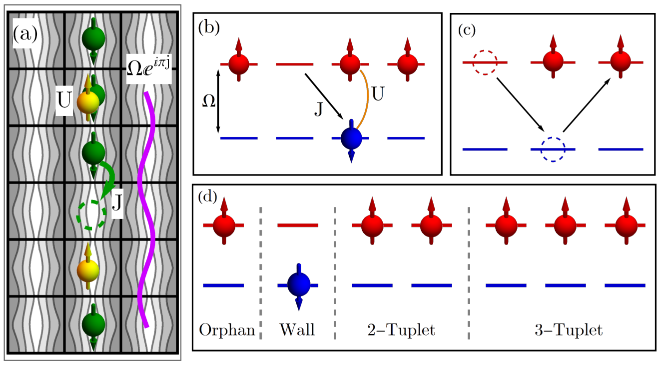

FIG. 1. (a) Schematic of Fermi-Hubbard optical lattice setup, confined to 1D, driven by an SOC-inducing laser with relative phase π between sites. (b) Resonance-assisted atomic motion in the gauged frame. An $\uparrow$ atom can tunnel into a neighbouring site already holding an $\uparrow$ atom, flipping its spin and creating a doublon. All other tunneling processes are off-resonant. (c) Leap-frog motion of two $\uparrow$ atoms. (d) Few-body structures present in a sparsely filled lattice. Orphans cannot move on their own, but interact with other atoms. Walls inhibit all motion and cannot move. 2-tuplets move freely via the leap-frog mechanism. 3-tuplets can shoot off a 2-tuplet, but exhibit nontrivial three-body dynamics.

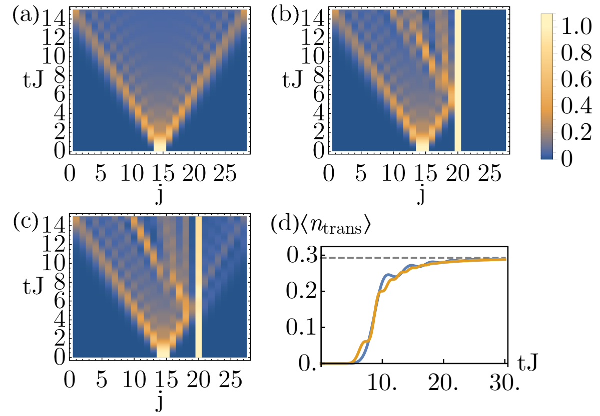

FIG. 2. (a) Dynamics of an initial 2-tuplet (using Eq. (2)). We plot atomic density $\langle \hat{n}_j \rangle$ (color scaled to emphasize features). (b) Reflection of a propagating 2-tuplet off a wall ($\downarrow$ singlon). (c) Collision of a propagating 2-tuplet with an orphan ($\uparrow$ singlon). Three-body dynamics cause non-reciprocal transmission and reflection. (d) Number of atoms transmitted past the orphan during the collision in panel (c). The orange line is direct Fermi-Hubbard numerics. The blue line uses a Kronecker delta potential single-particle scattering of strength $U_\delta = 2J$, which has an asymptotic value of $\langle \hat{n}_{\text{trans}} \rangle = 1 - 1/\sqrt{2}$ indicated in gray (see discussion of scattering in text).

$\hat{H}_0/\hbar = -J\sum_{\langle i,j\rangle,\sigma}(\hat{c}^\dagger_{i,\sigma}\hat{c}_{j,\sigma} + h.c.) + U\sum_j \hat{n}_{j,e}\hat{n}_{j,g}$ is the Fermi-Hubbard model (nearest-neighbour tunneling), and $\hat{H}_\Omega/\hbar = \frac{\Omega}{2}\sum_j(-1)^j(\hat{c}^\dagger_{j,e}\hat{c}_{j,g} + h.c.)$ is the laser drive. Here, $\hat{c}_{j,\sigma}$ annihilates an atom of spin $\sigma \in \{g, e\}$ on site j, and $\hat{n}_{j,\sigma} = \hat{c}^\dagger_{j,\sigma}\hat{c}_{j,\sigma}$. The lattice tunneling rate is J, and the onsite repulsion is U. The laser drive has Rabi frequency Ω and a site-dependent phase $e^{ij\pi} = (-1)^j$ arising from a mismatch between the driving and confining laser wavelengths, generating spin-orbit coupling (SOC) [5–7]. Every adjacent pair of sites has a relative phase of π, resulting in a relative minus sign between their laser couplings. Fig. 1(a) depicts the setup.

We define two new species of fermion, $\hat{a}_{j,\uparrow} = [\hat{c}_{j,e} + (-1)^j\hat{c}_{j,g}]/\sqrt{2}$ and $\hat{a}_{j,\downarrow} = [\hat{c}_{j,e} - (-1)^j\hat{c}_{j,g}]/\sqrt{2}$, for which the Hamiltonian becomes

$$\begin{aligned}\hat{H}/\hbar =& -J\sum_{\langle i,j\rangle}\left(\hat{a}^\dagger_{i,\uparrow}\hat{a}_{j,\downarrow} + h.c.\right)\\ &+ U\sum_j \hat{n}_{j,\uparrow}\hat{n}_{j,\downarrow} + \frac{\Omega}{2}\sum_j(\hat{n}_{j,\uparrow} - \hat{n}_{j,\downarrow}),\end{aligned} \tag{1}$$

with number operators $\hat{n}_{j,\sigma'} = \hat{a}^\dagger_{j,\sigma'}\hat{a}_{j,\sigma'}$ for new pseudo-spin states $\sigma' \in \{\uparrow, \downarrow\}$. The laser drive in this frame acts as an effective magnetic field. Tunneling is accompanied by a spin-flip due to the SOC. Direct tunneling into empty sites must cross an energy gap $\pm\Omega$, and is inhibited for strong driving $\Omega/J \gg 1$.

However, if we tune the drive strength to match the repulsion $U = \Omega$, an $\uparrow$ atom can tunnel into a site already holding an $\uparrow$ atom by flipping its spin and creating a doublon (two atoms of opposite spin). The energy loss $-\Omega$ is resonantly compensated by an energy gain U from repulsion, with total cost $-\Omega + U = 0$ allowing the process to occur freely at rate J. A $\downarrow$ atom tunneling into a site with another $\downarrow$ atom would instead cost $+\Omega + U = 2U$, and still be inhibited. Since tunneling into an already-occupied state is Pauli-blocked, the process described is the only one that can occur. In the limit $U/J = \Omega/J \to \infty$, we thus reduce the Hamiltonian to a density-dependent tunneling model (up to J/U corrections),

$$\hat{H}_\infty/\hbar = -J\sum_{\langle i,j\rangle}\hat{n}_{j,\uparrow}(1 - \hat{n}_{i,\downarrow})\left(\hat{a}^\dagger_{j,\downarrow}\hat{a}_{i,\uparrow} + h.c.\right), \tag{2}$$

where the number terms ensure that the spin-flip tunneling has an $\uparrow$ atom on the destination and no $\downarrow$ atom on the origin. This model is valid for timescales $tJ \lesssim U/J$, see Supplementary E [54] for benchmarking.

The constrained motion is depicted in Fig. 1(b), and can be understood as a leap-frog mechanism alternating between doublons and neighbouring $\uparrow$ singlons (single atoms). Assuming a sparse lattice with $N/L \ll 1$, we categorize the behaviour of few-atom configurations in Fig. 1(c). An $\uparrow$ singlon is an orphan, which cannot move on its own but will interact with other atoms. A $\downarrow$ singlon can neither move nor permit motion through itself, acting as a wall. A 2-tuplet (two adjacent $\uparrow$ singlons) moves freely via the leap-frog mechanism. A 3-tuplet (three adjacent $\uparrow$ singlons) can also move by shooting off a 2-tuplet, but exhibits nontrivial three-body dynamics that we discuss below.

In Fig. 2, we compare the density $\langle \hat{n}_j \rangle = \langle \hat{n}_{j,\uparrow} \rangle + \langle \hat{n}_{j,\downarrow} \rangle$ profiles of a 2-tuplet propagating freely (a), colliding with a wall (b), and with an orphan (c). The 2-tuplet acts as a quasiparticle that spreads ballistically, with wavefronts rising from an underlying quantum walk. Upon colliding with the orphan, we find that a nontrivial scattering process takes place. Some atom density $\langle \hat{n}_{\rm trans} \rangle = \sum_{j>j_0} \langle \hat{n}_j \rangle$ (j_0 the position of the orphan) is transmitted by forming a new 2-tuplet with the orphan, while some is reflected. The orphan acts as an effective scatterer whose own position is changed only if transmission occurs. The underlying reason for this outcome is tied to the self-localization properties of the three-atom system.

3-Tuplet bound states. The core dynamics for three atoms can be understood by considering a 3-tuplet. Fig. 3(a) shows the states that it can tunnel into. An atom can either tunnel into the middle, yielding stuck states that cannot move further, or out from the middle to make a 2-tuplet free to propagate. The 3-tuplet state thus has connectivity $\nu = 4$, which counts the number of Fock states that $\hat{H}$ couples it to. If we allow a 2-tuplet to propagate, an immobile orphan is generated, and the resulting state is reduced to connectivity $\nu = 2$.

This reduced connectivity lets us map the motion of the 3-tuplet to a 1D tight-binding chain with impurities. The accessible Fock states are left- and right-side 2-tuplet states, as shown in Fig. 3(a). We associate each of these states with a virtual lattice coordinate m (one for the doublon configuration, and one for neighbouring singlons), with two virtual sites m for every real site j. The 3-tuplet acts as a central site coupling to the left- and right-chains of states. In addition, it also couples to the two stuck states, acting as extra dead-end links. This model is analogous to a non-interacting Anderson impurity model (c.f. Supplementary A [54]),

$$\hat{H}^{(3)}/\hbar = -J \sum_{\langle m,n \rangle} \left(\hat{d}^\dagger_m \hat{d}_n + h.c. \right) - J \left(\hat{d}^\dagger_0 \hat{d}_L + \hat{d}^\dagger_0 \hat{d}_R + h.c. \right), \tag{3}$$

where $\hat{d}_m$ annihilates a fermion on virtual site m, $\hat{d}_0$ on the 3-tuplet, and $\hat{d}_L$, $\hat{d}_R$ on the stuck states (acting as impurities). The Anderson impurity model is known to host bound states, and indeed, we observe their presence in our system as well. Fig. 3(b) shows the density dynamics for an initial 3-tuplet. In contrast to the 2-tuplet, more than 2/3rds of the atoms remain in the sites they started in; see Fig. 3(c), where $\langle \hat{n}^{(N)}_{\rm init} \rangle$ is the total atom number summing over the N initially-filled sites. The 3-tuplet has overlap with exponentially localized bound eigenstates, and the corresponding population will not decrease as the system evolves. We find two such bound eigenstates, $\hat{H}_\infty |\phi^{(3)}_\pm\rangle = \pm\hbar E |\phi^{(3)}_\pm\rangle$ (up to exponentially small boundary corrections), with energy $E = \sqrt{2}bJ$ where $b^2 = 1 + \sqrt{2}$ is the wavefunction localization length in units of the real lattice spacing (see Supplementary A [54] for analytic forms of the eigenstates). In the limit $L \to \infty$, the 3-tuplet $|\uparrow,\uparrow,\uparrow\rangle$ has overlap $|\langle \uparrow,\uparrow,\uparrow |\phi^{(3)}_\pm\rangle|^2 = 1/(2\sqrt{2})$ with each bound eigenstate. Each of these eigenstates has $\langle \hat{n}^{(3)}_{\rm init,\pm} \rangle = 2 + 1/\sqrt{2}$ atoms on the initially-occupied sites [Fig. 3(c) inset]. We then find that a 3-tuplet should have $\langle \hat{n}^{(3)}_{\rm init} \rangle \approx 2.2$ atoms localized in the long-time limit, which matches direct numerics in Fig. 3(c).

This self-localization shows a stark difference between open and periodic boundary conditions, as evident from the density of an initial 3-tuplet over longer timescales [Figs. 3(d-e)]. For periodic boundaries, the 3-tuplet position eventually dissolves, as a 2-tuplet can wrap around the lattice and collide with the orphan from the opposite side. If another 2-tuplet then shoots off, now involving the old orphan, the new orphan will have moved outside the initial three sites. The timescale for this dissolving process grows with system size, since 2-tuplets must cross the entire lattice. For open boundaries, the 2-tuplets can only rebound off the wall and come back, allowing localization to persist. This is indicative of the presence of quantum few-body scars [62], as the system exhibits closed trajectories with reduced dimension of accessible Hilbert space size changing the long-time behaviour.

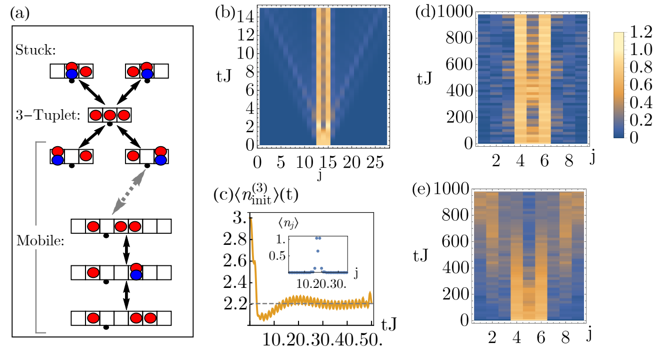

FIG. 3. (a) Schematic for a 3-tuplet's motion. Red and blue circles are ↑, ↓ atoms respectively. The 3-tuplet can tunnel into four states: Two stuck states, and two mobile (scattering) states that shoot off a 2-tuplet. The dots under the boxes indicate the center of the 3-tuplet. (b) Density dynamics for an initial 3-tuplet. (c) Number of atoms that stay in the initial three sites. The gray dashed line marks the analytic prediction of $\langle \hat{n}^{(3)}_{\rm init} \rangle \approx 2.2$ (c.f. Supplementary A [54]). The inset shows the density profile for the 3-tuplet bound eigenstates $|\phi^{(3)}_\pm\rangle$ (equal for both). (d-e) 3-Tuplet density dynamics for long times $tJ \gg 1$ (coarse-grained in time), for a small lattice using open (d) and periodic (e) boundaries. The periodic boundaries eventually dissolve the localization by wrapping 2-tuplets around to pull the orphan away.

The multi-body self-localization shown in Fig. 3 can be interpreted as a coherent quantum version of entropic confinement, where the system tends to stay in states with higher connectivity ν to reduce its kinetic energy. This is analogous to the three-body bound-states described by Efimov physics, although the system itself is quite different. While the higher energy scales in the system ($U = \Omega$) are not present in the effective Hamiltonian, they manifest indirectly by energetically enforcing restrictions on the motion. Localization is also present in higher-order N-tuplet structures (N neighbouring ↑ singlons), as seen in Fig. 4. We find that even-N configurations will smear out quickly, while odd-N configurations exhibit long-time localization for similar reasons (c.f. Supplementary B [54]).

Scattering. We can use the intuitions developed above to understand the 2-tuplet and orphan scattering in Figs. 2(c-d). As discussed in the previous section and Supplementary A [54], the Hamiltonian for 3-tuplets can be reduced to

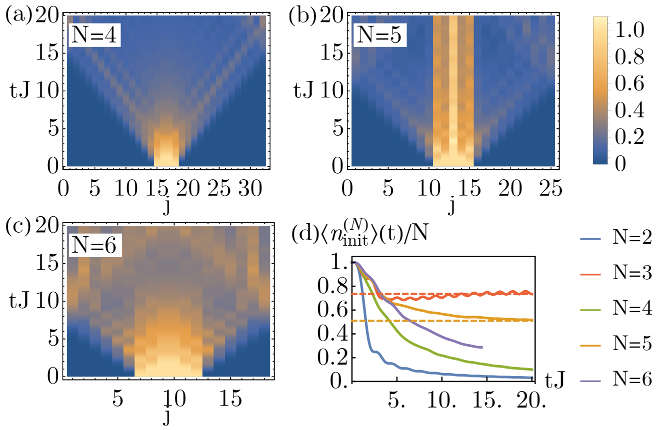

FIG. 4. Density dynamics of an N-tuplet of $\uparrow$ atoms, for $N = 4$ (a), $N = 5$ (b) and $N = 6$ (c). Localization persists for odd $N = 5$, but not the even cases. (d) Total number of remaining atoms in the initially-populated sites, for $N = 2, 3, 4, 5, 6$. System sizes are $L = 36, 35, 32, 25, 18$. The red dashed line is the analytic prediction for $N = 3$ (c.f. Supplementary A [54]). The orange dashed line is a quasi-numeric prediction from a bound-state search for $N = 5$ (c.f. Supplementary B [54]). The even lines are expected to stabilize at mean density N/L in the long-time limit. Note that the $N = 6$ line is stopped early to avoid rebounds from the edges.

a tight-binding chain with a single impurity state shifted in energy (though there are two stuck states, one linear combination decouples). We can further remodel the scattering as a single-particle problem, with a quasiparticle (corresponding to a 2-tuplet) moving though a kronecker-delta potential formed by the impurity (corresponding to an orphan). Under this picture, Eq. (3) can be rewritten as $\hat{H}^{(3)}_{\text{eff}}/\hbar = -J \sum_{\langle m,n \rangle} \left(\hat{d}^\dagger_m \hat{d}_n + h.c. \right) - U_\delta \hat{d}^\dagger_0 \hat{d}_0$ for a potential depth U_δ. We estimate the transmission by initializing a particle at $m_{\text{init}} < 0$ and evaluating its density at all $m > 0$ for times $tJ \gtrsim |m_{\text{init}}|$, rescaling the time and amplitude by 2 (since a 2-tuplet takes two steps to move one real lattice site, and has two atoms).

Fig. 2(d) compares this estimated transmission amplitude with direct three-atom numerics. With a potential depth of $U_\delta = 2J$, corresponding to the same bound-state localization length b in the single- and three-particle problems, we find good agreement. This simplification also lets us find an analytic expression for the transmission, yielding $\langle \hat{n}_{\text{trans}} \rangle = 1 - 1/\sqrt{2} \approx 0.29$ (c.f. Supplementary C [54]). The agreement in Fig. 2(d) showcases the reduction of a three-body interacting problem to that of a single particle with tractable emergent interactions.

The nontrivial feature not captured by this mapping is the non-reciprocal position dependence of the scatterer. Consider an orphan initially on the right of the three sites of an imminent collision. If the 2-tuplet reflects, then the orphan remains in place. If transmission occurs, then a new 2-tuplet shoots off to the right, leaving a new orphan two sites left of the original orphan's location. The system exhibits non-reciprocal behaviour where the scatterer is shifted by two sites upon transmission, but not upon reflection. In a classical description, its effective mass is infinite for reflection but finite (and set by quantized motion) for transmission. This behavior is evident in the vertical stripe of atomic density two sites left of the orphan in Fig. 2(c). Finding such non-reciprocal effects in a purely closed system as a consequence of interaction-induced constraints is an intriguing feature impossible to capture by the Anderson mapping in Eq. (3).

Experimental implementations. Realizing this system is straightforward with a 3D optical lattice populated by two-level atoms. A suggested implementation with e.g. ^{87}Sr is to set the confinement to $V_x \sim 8$–$20 E_R$, and $V_y, V_z \gtrsim 100 E_R$ (with E_R the lattice recoil energy), such that on-site repulsion satisfies $U/J \sim 30$–500 [63]. The dynamical timescale will then be set by $J \sim 10$–$100 \times 2\pi$ Hz. To generate the desired SOC one could use an optical transition in alkaline-earth atoms, or a Raman transitions in alkali atoms. In both cases, it is required that the laser-imparted phase along $\hat{x}$ is π per lattice site. A coherence time much longer than the one set by J is also required. This condition is much more favorable that the stringent condition required to observe superexchange interactions (set by J^2/U).

Measurement and preparation of the few-body atomic structures are easiest to do with quantum gas microscopes and optical tweezers respectively. However, a state-of-the-art optical lattice clock such as the ^{87}Sr clock [64, 65] can also probe the 3-tuplet localization without single-site resolution. A sparse configuration of many 3-tuplets can be generated with a lattice tilt and a pulse sequence capable of spectroscopically resolving a specific set of transitions (c.f. Supplementary D [54]). Allowing the system to evolve and then undoing the pulse sequence to detect the percentage of the atoms remaining in the initial triply-occupied sites can be used to verify localization.

Conclusions and outlook. We have proposed a simple and intuitive system where spin-orbit coupling and interactions generate constrained dynamics. This system exhibits features of self-localization and non-reciprocity, and maps to non-interacting models while maintaining nontrivial lattice effects. A vast number of extensions can be considered, especially if one looks to higher densities or higher dimensions. At higher densities, $\downarrow$ singlons will act as bottlenecks, generically producing many-body quantum scars. Even with no $\downarrow$ singlons, a transfer matrix calculation analogous to [66] reveals that in the thermodynamic limit there will be an exponentially large subspace of 2^L product states which will be eigenstates of the dynamics, and hence perfect many-body quantum scars (c.f. Supplementary F [54]). The system is also simple to generalize to higher dimensions, needing only an SOC drive with a π phase along all allowed directions. The underlying physics can be connected to dynamical gauge fields, where atomic motion by one species is influenced by another in a non-reciprocal manner [21, 24, 26]. Higher filling fractions lead to long-range doublon correlations, which can be relevant to studies of superconductivity. Fermionic statistics will also play a significant role in higher dimensions and interplay with the scar and non-reciprocity features. The accessible implementation and the rich breadth of physics displayed make the proposed setup an ideal playground for future investigations.

Acknowledgements M.M. acknowledges support from a CTQM graduate fellowship. I.K. was supported by a National Research Council Fellowship through the National Institute of Standards and Technology. R.M.N. was supported by the AFOSR grant FA9550-17-1-0183. A.M.R is supported by the AFOSR grant FA9550-18-1-0319 and its MURI Initiative, by the DARPA and ARO grant W911NF-16-1-0576, the DARPA DRINQs grant, the ARO single investigator award W911NF-19-1-0210, the NSF PHY1820885, NSF JILA-PFC PHY1734006 grants, and by NIST.

* mikhail.mamaev@colorado.edu

[1] Immanuel Bloch, Jean Dalibard, and Sylvain Nascimbene. Quantum simulations with ultracold quantum gases. *Nature Physics*, 8(4):267, 2012.

[2] K Osterloh, M Baig, L Santos, P Zoller, and M Lewenstein. Cold atoms in non-abelian gauge potentials: from the hofstadter" moth" to lattice gauge theory. *Physical review letters*, 95(1):010403, 2005.

[3] Immanuel Bloch, Jean Dalibard, and Wilhelm Zwerger. Many-body physics with ultracold gases. *Reviews of modern physics*, 80(3):885, 2008.

[4] Eduardo Fradkin and Stephen H Shenker. Phase diagrams of lattice gauge theories with higgs fields. *Physical Review D*, 19(12):3682, 1979.

[5] Michael L. Wall, Andrew P. Koller, Shuming Li, Xibo Zhang, Nigel R. Cooper, Jun Ye, and Ana Maria Rey. Synthetic Spin-Orbit Coupling in an Optical Lattice Clock. *Physical Review Letters*, 116(3):035301, January 2016.

[6] S. Kolkowitz, S. L. Bromley, T. Bothwell, M. L. Wall, G. E. Marti, A. P. Koller, X. Zhang, A. M. Rey, and J. Ye. Spin-orbit-coupled fermions in an optical lattice clock. *Nature*, 542(7639):66, December 2016.

[7] M Eric Tai, Alexander Lukin, Matthew Rispoli, Robert Schittko, Tim Menke, Dan Borgnia, Philipp M Preiss, Fabian Grusdt, Adam M Kaufman, and Markus Greiner. Microscopy of the interacting harper–hofstadter model in the two-body limit. *Nature*, 546(7659):519, 2017.

[8] SL Bromley, S Kolkowitz, T Bothwell, D Kedar, A Safavi-Naini, ML Wall, C Salomon, AM Rey, and J Ye. Dynamics of interacting fermions under spin–orbit coupling in an optical lattice clock. *Nature Physics*, page 1, 2018.

[9] Monika Aidelsburger, Marcos Atala, Michael Lohse, Julio T Barreiro, B Paredes, and Immanuel Bloch. Realization of the hofstadter hamiltonian with ultracold atoms in optical lattices. *Physical review letters*, 111(18):185301, 2013.

[10] Florian Meinert, Manfred J Mark, Emil Kirilov, Katharina Lauber, Philipp Weinmann, Michael Gröbner, Andrew J Daley, and Hanns-Christoph Nägerl. Observation of many-body dynamics in long-range tunneling after a quantum quench. *Science*, 344(6189):1259–1262, 2014.

[11] Hirokazu Miyake, Georgios A Siviloglou, Colin J Kennedy, William Cody Burton, and Wolfgang Ketterle. Realizing the harper hamiltonian with laser-assisted tunneling in optical lattices. *Physical review letters*, 111(18):185302, 2013.

[12] Jonathan Simon, Waseem S Bakr, Ruichao Ma, M Eric Tai, Philipp M Preiss, and Markus Greiner. Quantum simulation of antiferromagnetic spin chains in an optical lattice. *Nature*, 472(7343):307, 2011.

[13] Ole Jürgensen, Florian Meinert, Manfred J Mark, Hanns-Christoph Nägerl, and Dirk-Sören Lühmann. Observation of density-induced tunneling. *Physical review letters*, 113(19):193003, 2014.

[14] H Lignier, Carlo Sias, Donatella Ciampini, Y Singh, A Zenesini, O Morsch, and Ennio Arimondo. Dynamical control of matter-wave tunneling in periodic potentials. *Physical review letters*, 99(22):220403, 2007.

[15] Florian Meinert, Manfred J Mark, Katharina Lauber, Andrew J Daley, and H-C Nägerl. Floquet engineering of correlated tunneling in the bose-hubbard model with ultracold atoms. *Physical review letters*, 116(20):205301, 2016.

[16] Julian Struck, Christoph Ölschläger, R Le Targat, Parvis Soltan-Panahi, André Eckardt, Maciej Lewenstein, Patrick Windpassinger, and Klaus Sengstock. Quantum simulation of frustrated classical magnetism in triangular optical lattices. *Science*, 333(6045):996–999, 2011.

[17] Gregor Jotzu, Michael Messer, Rémi Desbuquois, Martin Lebrat, Thomas Uehlinger, Daniel Greif, and Tilman Esslinger. Experimental realization of the topological haldane model with ultracold fermions. *Nature*, 515(7526):237, 2014.

[18] Logan W Clark, Brandon M Anderson, Lei Feng, Anita Gaj, Kathryn Levin, and Cheng Chin. Observation of density-dependent gauge fields in a bose-einstein condensate based on micromotion control in a shaken two-dimensional lattice. *Physical review letters*, 121(3):030402, 2018.

[19] Michael Messer, Kilian Sandholzer, Frederik Görg, Joaquín Minguzzi, Rémi Desbuquois, and Tilman Esslinger. Floquet dynamics in driven fermi-hubbard systems. *Physical review letters*, 121(23):233603, 2018.

[20] Frederik Görg, Michael Messer, Kilian Sandholzer, Gregor Jotzu, Rémi Desbuquois, and Tilman Esslinger. Enhancement and sign change of magnetic correlations in a driven quantum many-body system. *Nature*, 553(7689):481, 2018.

[21] Debasish Banerjee, M Dalmonte, M Müller, E Rico, P Stebler, U-J Wiese, and P Zoller. Atomic quantum simulation of dynamical gauge fields coupled to fermionic matter: From string breaking to evolution after a quench. *Physical review letters*, 109(17):175302, 2012.

[22] Alejandro Bermudez, Tobias Schaetz, and Diego Porras. Synthetic gauge fields for vibrational excitations of trapped ions. *Physical review letters*, 107(15):150501, 2011.

[23] Philipp Hauke, Olivier Tieleman, Alessio Celi, Christoph Ölschläger, Juliette Simonet, Julian Struck, Malte Weinberg, Patrick Windpassinger, Klaus Sengstock, Maciej Lewenstein, et al. Non-abelian gauge fields and topological insulators in shaken optical lattices. *Physical review letters*, 109(14):145301, 2012.

[24] Luca Barbiero, Christian Schweizer, Monika Aidelsburger, Eugene Demler, Nathan Goldman, and Fabian Grusdt. Coupling ultracold matter to dynamical gauge fields in optical lattices: From flux-attachment to z2 lattice gauge theories. *arXiv preprint arXiv:1810.02777*, 2018.

[25] Frederik Görg, Kilian Sandholzer, Joaquín Minguzzi, Rémi Desbuquois, Michael Messer, and Tilman Esslinger. Realisation of density-dependent peierls phases to couple dynamical gauge fields to matter. *arXiv preprint arXiv:1812.05895*, 2018.

[26] Christian Schweizer, Fabian Grusdt, Moritz Berngruber, Luca Barbiero, Eugene Demler, Nathan Goldman, Immanuel Bloch,

and Monika Aidelsburger. Floquet approach to $\mathbb{Z}_2$ lattice gauge theories with ultracold atoms in optical lattices. *arXiv preprint arXiv:1901.07103*, 2019.

[27] Chester P Rubbo, Salvatore R Manmana, Brandon M Peden, Murray J Holland, and Ana Maria Rey. Resonantly enhanced tunneling and transport of ultracold atoms on tilted optical lattices. *Physical Review A*, 84(3):033638, 2011.

[28] VV Ivanov, A Alberti, M Schioppo, G Ferrari, MLCM Artoni, ML Chiofalo, and GM Tino. Coherent delocalization of atomic wave packets in driven lattice potentials. *Physical review letters*, 100(4):043602, 2008.

[29] Alessandro Zenesini, Hans Lignier, Donatella Ciampini, Oliver Morsch, and Ennio Arimondo. Coherent control of dressed matter waves. *Physical review letters*, 102(10):100403, 2009.

[30] André Eckardt. Colloquium: Atomic quantum gases in periodically driven optical lattices. *Reviews of Modern Physics*, 89(1):011004, 2017.

[31] Philipp M Preiss, Ruichao Ma, M Eric Tai, Alexander Lukin, Matthew Rispoli, Philip Zupancic, Yoav Lahini, Rajibul Islam, and Markus Greiner. Strongly correlated quantum walks in optical lattices. *Science*, 347(6227):1229–1233, 2015.

[32] Alessio Lerose, Bojan Žunkovič, Alessandro Silva, and Andrea Gambassi. Quasilocalized excitations induced by long-range interactions in translationally invariant quantum spin chains. *Physical Review B*, 99(12):121112, 2019.

[33] M. Mamaev, R. Blatt, J. Ye, and A. M. Rey. Cluster state generation with spin-orbit coupled fermionic atoms in optical lattices. *Physical review letters*, 122:160402, 2019.

[34] Philip Warren Anderson. Localized magnetic states in metals. *Physical Review*, 124(1):41, 1961.

[35] Alexander Cyril Hewson. *The Kondo problem to heavy fermions*, volume 2. Cambridge university press, 1997.

[36] Stefan K Kehrein and Andreas Mielke. Theory of the anderson impurity model: the schrieffer–wolff transformation reexamined. *annals of physics*, 252(1):1–32, 1996.

[37] László Deák and Tamás Fülöp. Reciprocity in quantum, electromagnetic and other wave scattering. *Annals of Physics*, 327(4):1050–1077, 2012.

[38] Naoto Shiraishi and Takashi Mori. Systematic construction of counterexamples to the eigenstate thermalization hypothesis. *Physical review letters*, 119(3):030601, 2017.

[39] Sanjay Moudgalya, Stephan Rachel, B Andrei Bernevig, and Nicolas Regnault. Exact excited states of nonintegrable models. *Physical Review B*, 98(23):235155, 2018.

[40] CJ Turner, AA Michailidis, DA Abanin, M Serbyn, and Z Papic. Weak ergodicity breaking from quantum many-body scars. *Nature Physics*, 14(7):745–749, 2018.

[41] Vitaly Efimov. Energy levels arising from resonant two-body forces in a three-body system. *Physics Letters B*, 33(8):563–564, 1970.

[42] Pascal Naidon and Shimpei Endo. Efimov physics: a review. *Reports on Progress in Physics*, 80(5):056001, 2017.

[43] Zhe-Yu Shi, Xiaoling Cui, and Hui Zhai. Universal trimers induced by spin-orbit coupling in ultracold fermi gases. *Physical review letters*, 112(1):013201, 2014.

[44] Tatjana Gericke, Peter Würtz, Daniel Reitz, Tim Langen, and Herwig Ott. High-resolution scanning electron microscopy of an ultracold quantum gas. *Nature Physics*, 4(12):949, 2008.

[45] Waseem S Bakr, Jonathon I Gillen, Amy Peng, Simon Fölling, and Markus Greiner. A quantum gas microscope for detecting single atoms in a hubbard-regime optical lattice. *Nature*, 462(7269):74, 2009.

[46] Jacob F Sherson, Christof Weitenberg, Manuel Endres, Marc Cheneau, Immanuel Bloch, and Stefan Kuhr. Single-atom-resolved fluorescence imaging of an atomic mott insulator. *Nature*, 467(7311):68, 2010.

[47] Lawrence W Cheuk, Matthew A Nichols, Melih Okan, Thomas Gersdorf, Vinay V Ramasesh, Waseem S Bakr, Thomas Lompe, and Martin W Zwierlein. Quantum-gas microscope for fermionic atoms. *Physical review letters*, 114(19):193001, 2015.

[48] Ryuta Yamamoto, Jun Kobayashi, Takuma Kuno, Kohei Kato, and Yoshiro Takahashi. An ytterbium quantum gas microscope with narrow-line laser cooling. *New Journal of Physics*, 18(2):023016, 2016.

[49] Debayan Mitra, Peter T Brown, Elmer Guardado-Sanchez, Stanimir S Kondov, Trithep Devakul, David A Huse, Peter Schauss, and Waseem S Bakr. Quantum gas microscopy of an attractive fermi–hubbard system. *Nature Physics*, 14(2):173, 2018.

[50] Manuel Endres, Hannes Bernien, Alexander Keesling, Harry Levine, Eric R Anschuetz, Alexandre Krajenbrink, Crystal Senko, Vladan Vuletic, Markus Greiner, and Mikhail D Lukin. Atom-by-atom assembly of defect-free one-dimensional cold atom arrays. *Science*, 354(6315):1024–1027, 2016.

[51] MA Norcia, AW Young, and AM Kaufman. Microscopic control and detection of ultracold strontium in optical-tweezer arrays. *Physical Review X*, 8(4):041054, 2018.

[52] Alexandre Cooper, Jacob P Covey, Ivaylo S Madjarov, Sergey G Porsev, Marianna S Safronova, and Manuel Endres. Alkaline-earth atoms in optical tweezers. *Physical Review X*, 8(4):041055, 2018.

[53] Samuel Saskin, JT Wilson, Brandon Grinkemeyer, and JD Thompson. Narrow-line cooling and imaging of ytterbium atoms in an optical tweezer array. *Physical Review Letters*, 122(14):143002, 2019.

[54] See supplementary material for details, which includes refs. 55-61.

[55] Eleftherios N Economou. *Green's functions in quantum physics*, volume 3. Springer, 1983.

[56] Jun Ye, H. J. Kimble, and Hidetoshi Katori. Quantum State Engineering and Precision Metrology Using State-Insensitive Light Traps. *Science*, 320(5884):1734–1738, June 2008.

[57] A. Goban, R. B. Hutson, G. E. Marti, S. L. Campbell, M. A. Perlin, P. S. Julienne, J. P. D'Incao, A. M. Rey, and J. Ye. Emergence of multi-body interactions in a fermionic lattice clock. *Nature*, 563(7731):369, November 2018.

[58] Martin M Boyd. *High Precision Spectroscopy of Strontium in an Optical Lattice: Towards a New Standard for Frequency and Time*. PhD thesis, University of Colorado at Boulder, 2007.

[59] M. A. Perlin and A. M. Rey. Effective multi-body SU(N)-symmetric interactions of ultracold fermionic atoms on a 3D lattice. *New Journal of Physics*, 21(4):043039, April 2019.

[60] T. C. Li, H. Kelkar, D. Medellin, and M. G. Raizen. Real-time control of the periodicity of a standing wave: An optical accordion. *Optics Express*, 16(8):5465–5470, April 2008.

[61] S. Al-Assam, R. A. Williams, and C. J. Foot. Ultracold atoms in an optical lattice with dynamically variable periodicity. *Physical Review A*, 82(2):021604, August 2010.

[62] Eric J. Heller. Bound-state eigenfunctions of classically chaotic hamiltonian systems: Scars of periodic orbits. *Phys. Rev. Lett.*, 53:1515–1518, Oct 1984.

[63] X. Zhang, M. Bishof, S. L. Bromley, C. V. Kraus, M. S. Safronova, P. Zoller, A. M. Rey, and J. Ye. Spectroscopic observation of $\mathrm{SU}(n)$-symmetric interactions in sr orbital magnetism. *Science*, 345(6203):1467–1473, September 2014.

[64] Sara L Campbell, RB Hutson, GE Marti, A Goban, N Darkwah Oppong, RL McNally, L Sonderhouse, JM Robinson, W Zhang,

BJ Bloom, et al. A fermi-degenerate three-dimensional optical lattice clock. *Science*, 358(6359):90–94, 2017.

[65] Michael L Wall, Andrew P Koller, Shuming Li, Xibo Zhang, Nigel R Cooper, Jun Ye, and Ana Maria Rey. Synthetic spin-orbit coupling in an optical lattice clock. *Physical review letters*, 116(3):035301, 2016.

[66] Vedika Khemani and Rahul Nandkishore. Local constraints can globally shatter Hilbert space: a new route to quantum information protection. *arXiv e-prints*, page arXiv:1904.04815, Apr 2019.